Check for updates

Bilateral photocatalytic mechanism of dye degradation by a designed ferrocene-functionalized cluster under natural sunlight†

Kuan-Guan Liu,‡*[a] Farzaneh Rouhani,‡[b] Xue-Mei Gao,‡[a] Mahsa Abbasi-Azad,[b] Jing-Zhe Li,[a] Xiu-De Hu,[a] Wei Wang,[a] Mao-Lin Hu*[c] and Ali Morsali [iD]*[b]

Extensive composition engineering research has been conducted on bandgap tunability, but the combination of two mechanisms for better photon harvesting over a wide range has rarely happened; this is of great importance for improving photocatalytic efficiency with sunlight. In order to enable concurrent heterogenic Fenton and Fenton-like reactions for dye degradation, two novel ferrocene-functionalized clusters, $[(PPh_3)_3CuO_2CFcCO_2Cu(PPh_3)_3] \cdot 3CH_3OH$ (D_1) and $[(PPh_3)_2AgO_2CFcCO_2Ag(PPh_3)_2]_2 \cdot 7CH_3OH$ (D_2) were designed, synthesized and characterized by multiple techniques. These chemically and thermally stable coinage clusters exhibit high photocatalytic activity towards the degradation of methylene blue as a model dye in the presence of H_2O_2 under direct sunlight irradiation. The degradation performance of complex D_1 is about twice that of complex D_2. The catalytic performance of D_1 (15 000 mg g^{-1} in less than 20 min) is superior to those of other reported complexes, which can be attributed to the high level of generated hydroxyl radicals which are the most active species for dye degradation in the combination of Fenton and Fenton-like mechanisms. In addition to the degradation carried out with the aid of the Fe(III) of ferrocene, based on the Fenton mechanism, the photogenerated holes trapped by Cu(I) act as catalysts in the Fenton-like mechanism to produce an excess of hydroxyl radicals, adding to those formed via scavenging of photogenerated electrons by hydrogen peroxide. Furthermore, the performance of D_1 in the presence of H_2O_2 as a dual photocatalyst under natural sunlight irradiation needs no pH adjustment which is a unique characteristic. This bilateral compound offers a promising strategy for the design of new photocatalysts.

Introduction

Dye-containing wastewater is increasing rapidly with industrial development, being discharged mainly from the textile, paper and print industries.[1,2] The stability of dye molecule structures makes them inert to destructive agents such as light, heat and oxidizing species. This means that treatment and dye decolorization have become enormous challenges.[3–6] Despite the use of various methods for wastewater treatment, new effective technologies are still required which offer sim-

[a] *State Key Laboratory of High-efficiency Coal Utilization and Green Chemical Engineering, Ningxia University, Yin-Chuan 750021, P. R. China.*
E-mail: liukuanguan@nxu.edu.cn
[b] *Department of Chemistry, Faculty of Sciences, Tarbiat Modares University, P.O. Box 14115-175, Tehran, Iran. E-mail: morsali_a@modares.ac.ir*
[c] *College of Chemistry and Materials Engineering, Wenzhou University, Wenzhou 325035, P. R. China. E-mail: maolin_hu@yahoo.com*
† Electronic supplementary information (ESI) available. CCDC 1947011 and 1947012. For ESI and crystallographic data in CIF or other electronic format see DOI: 10.1039/c9cy02003a
‡ These authors are contributed equally to this work.

plicity of design and operation to improve efficiency and economic utility; they also need to work with cheap resources.[7–12] Photocatalysis offers the possibility of employing sustainable and abundant solar energy to promote treatment in mild conditions, and so has attracted much attention for wastewater treatment.[13–16] Semi-conductors for the Fenton mechanism that produce ˙OH from the reaction between ferrous salts and H_2O_2 have been used effectively for decolorizing soluble and insoluble dyes.[17,18] However, in a traditional Fenton reaction, only a small proportion of the H_2O_2 is transformed into an effective oxidant to convert the recalcitrant contaminants,[19–21] which has led to increasing H_2O_2 utilization and recycling of used Fe^{2+}. Typical disadvantages of the homogeneous Fenton process include its high utilization of chemical agents, its limited usable pH range, the negative effects of some complex agents like phosphate anions, and the significant amounts of produced sludge.[22,23] Ferrocene (Fc) as an organic transition metal compound, which is non-toxic, insoluble and highly stable in water due to the electron donor–acceptor conjugated structure, has been widely used in many fields especially as a heterogeneous Fenton catalyst. However, limited studies have

This journal is © The Royal Society of Chemistry 2020

Catal. Sci. Technol., 2020, **10**, 757–767 | 757

been conducted on the applications of such a conjugated structure in heterogeneous Fenton-like processes.[24–27] Most of the previous studies have focused on the use of heterogeneous Fenton systems for wastewater treatment by immobilization of Fc on silica, mesoporous materials, carbon nanotubes, MCM-48, and some other platforms.[16,28–31] On the other hand, the Cu ion is known as a reactant with H_2O_2 for the Fenton-like reaction, resulting in high production rates of OH radicals in a wide pH range and leading to a high rate of dye degradation, but limited studies have focused on the heterogeneous copper cluster as a photocatalyst.[32–34] In this work, for the first time, we designed and synthesized two similar Fc-functionalized coinage clusters (Ag and Cu) as bilateral photocatalysts utilizing Fenton and Fenton-like mechanisms for the degradation of a model dye, methylene blue (MB). UV-vis analysis demonstrated that these structures have a bandgap of about 2 eV and suitable conduction band (CB) and valence band (VB) positions for the degradation of the model dye in sunlight. The results showed that the degradation of the model dye with the compound containing Fc and copper is much faster and more effective than the structure containing silver. As far as we know, D_1 which uses the combination of Fenton and Fenton-like mechanisms is the fastest and the most effective photocatalyst reported for MB degradation. Furthermore, this catalyst works in sunlight and does not require any pH adjustment.

Experimental

Synthesis of $[(PPh_3)_3CuO_2CFcCO_2Cu(PPh_3)_3]\cdot3CH_3OH$ (D$_1$)

Cu_2O (0.0429 g, 0.3 mmol) was dissolved in a mixture of 0.5 mL of $NH_3\cdot H_2O$ and 6 mL of methanol with ultrasonic irradiation. The obtained colorless solution became a pea-green turbid solution after the addition of 0.3 mmol (0.082 g) of $Fc(COOH)_2$. Then an equal amount of triphenylphosphine (0.078 g, 0.3 mmol) was added to the obtained solution. The sandy-brown suspension was sealed and heated to 70 °C for 20 hours. It was then filtered after cooling to room temperature. Slow evaporation of the solution produced the product as brown-yellow crystals. Yield: *ca.* 93.3 mg, 46.5%.

Synthesis of $[(PPh_3)_2AgO_2CFcCO_2Ag(PPh_3)_2]_2\cdot7CH_3OH$ (D$_2$)

Ag_2O (0.0695 g, 0.3 mmol) was dissolved in a mixture of 0.5 mL of $NH_3\cdot H_2O$ and 6 mL of methanol with ultrasonic irradiation. The obtained colorless solution became brown after the addition of 0.3 mmol (0.082 g) of $Fc(COOH)_2$. Then an equal amount of triphenylphosphine (0.078 g, 0.3 mmol) was added to the solution. The sandy-brown suspension was sealed and heated to 70 °C for 20 hours. Slow evaporation of the filtered solution produced the product as orange crystals. Yield: *ca.* 65.8 mg, 53.7%.

General procedure for dye degradation

150 ml of an aqueous solution containing 1000 ppm of MB was prepared as a dye model, and 10 mg of photocatalyst and 100 µL of fresh H_2O_2 were added to the mixture. The mixture was exposed to sunlight and 3 mL aliquots were collected every 5 min for UV-visible analysis. After complete discoloration of the mixture, the photocatalyst was centrifuged, washed with water and dried at 80 °C for reusability tests.

Results and discussion

Characterization and crystal structure of $[(PPh_3)_3CuO_2CFcCO_2Cu(PPh_3)_3]\cdot3CH_3OH$ (D$_1$)

Under ultrasonication, Cu_2O was dissolved in a mixture of $NH_3\cdot H_2O$ and methanol which resulted in the formation of a colorless solution. Equimolar amounts of $Fc(COOH)_2$ and triphenylphosphine were added to the solution. The sandy-brown suspension was heated to 70 °C for 20 hours after sealing. Subsequent slow evaporation of the solution provided brown-yellow crystals of D_1 with an average yield. D_1 is air and water stable, which are important factors for a water purification catalyst. The molecular structure of $[(PPh_3)_3CuO_2CFcCO_2Cu(PPh_3)_3]\cdot3CH_3OH$ (D$_1$) is shown in Fig. 1. The D_1 structure crystallizes as a trinuclear cluster in the orthorhombic space group (*Pbca*). The central Fc dicarboxylic acid is connected to two Cu(ı) centers through the oxygen of the carboxylic functional groups, and the Cu⋯O contacts range from 2.072 to 2.081 Å. Each copper atom is connected to three PPh_3 groups, and the Cu–P bond distances vary from 2.339 to 2.365 Å. The Tolman's cone angles in the PPh_3 moiety are in the range of 42.91 to 49.84 degrees and the torsion angles of the cyclopentadienyl rings vary from 100.67 to 103.93 degrees. Hydrogen bonding between hydrogens of the CH_3OH solvent and the free oxygen of the Fc dicarboxylic acid moiety lead to the presence of three methanol molecules in the structure. Altogether, the single-crystal X-ray structure analysis shows that the ferrocenyl group is placed at the core of the binuclear copper structure. Structural refinement and the crystallographic data with selected bond lengths and angles for the D_1 structure are provided in Tables S1 and S2,† respectively.

The IR spectrum of D_1 shows characteristic bands at around 3306, 3051, 1563, 1478–1433 and 1380–1342 cm^{-1} which can be attributed to the stretching frequencies of the C–H of phenyl groups, C–H bond of Fc, C=O of carbonyl groups, C=C of Fc, and characteristic bonds of PPh_3, consistent with the formulation (Fig. 2A). The thermal stability of D_1 was evaluated by thermogravimetric analysis (TGA). TGA on the synthesized sample indicates that the first weight-loss step can be attributed to the extraction of solvent molecules below 150 °C (calculated 4.66%, found approx. 5%). The principal weight-loss step occurs between 150 and 300 °C during the decomposition of the cluster (Fig. 2B). After that, about 10% weight remains (which corresponds to the metal section of the structure); the organic fraction entirely decomposes. Accordingly, the remaining portion could probably be $Cu_2O\cdot FeO$, but it should be noted that a further phase study on the residuals was not performed. The general weight loss in the temperature range of 150–300 °C of about 85% is near to the calculated
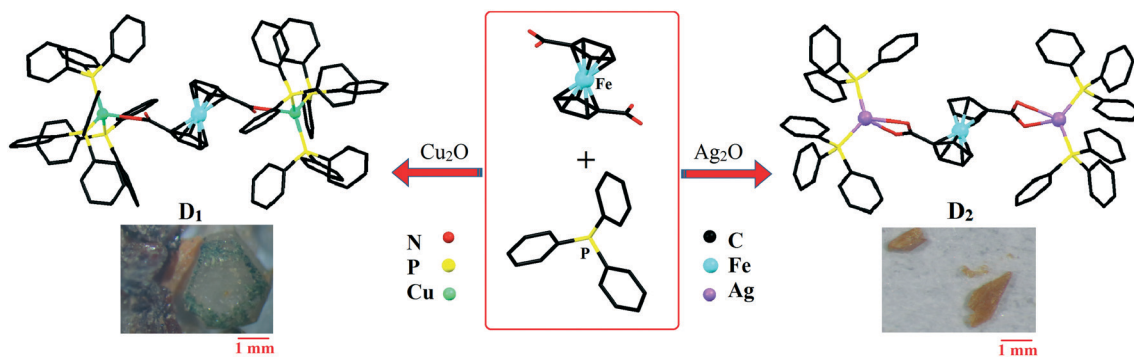
758 | *Catal. Sci. Technol.*, 2020, **10**, 757–767

This journal is © The Royal Society of Chemistry 2020

Fig. 1 Structural representations of D_1 and D_2 clusters.
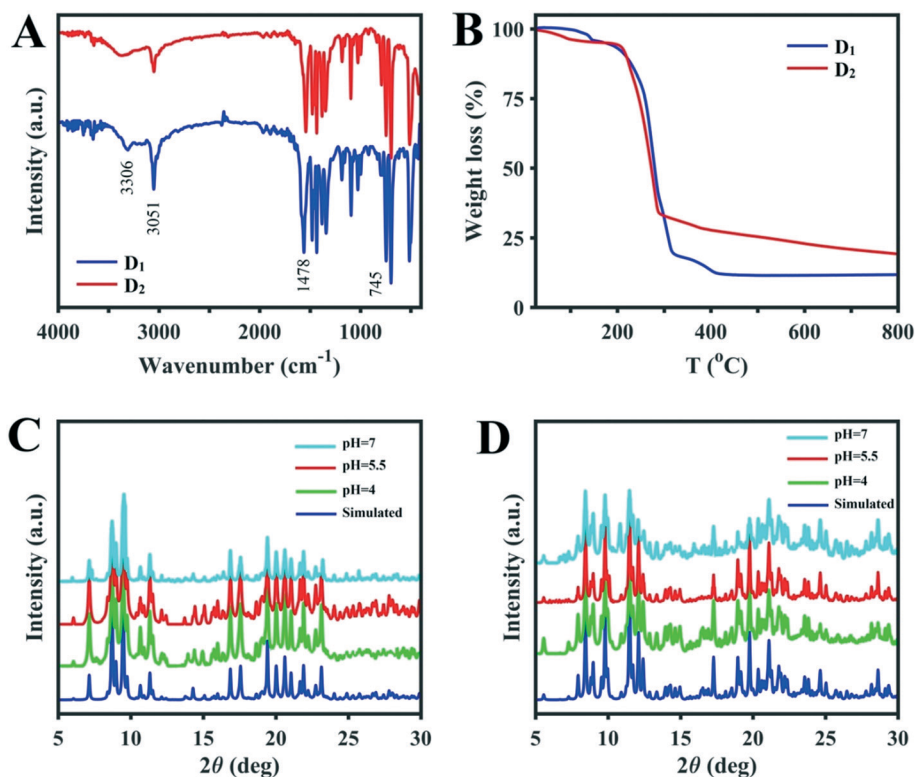

Fig. 2 (A) IR spectra and (B) TGA of D_1 and D_2. Comparisons of the simulated XRD patterns of (C) D_1 and (D) D_2 with samples immersed for 4 hours in solutions with various pH values.

amount of 79.5%. Accordingly, during the major weight-loss step, cluster D_1 fully decomposed to an uncertain metallic structure according to the TGA results. As a result, D_1 is sufficiently stable for use as a dye degradation photocatalyst with sunlight irradiation.

Characterization and crystal structure of $[(PPh_3)_2AgO_2CFcCO_2Ag(PPh_3)_2]_2\cdot7CH_3OH$ (D_2)

The synthesis steps for D_2 were the same as those for structure D_1, except that Ag_2O was used instead of Cu_2O. The molecular structure of $[(PPh_3)_2AgO_2CFcCO_2Ag(PPh_3)_2]_2\cdot7CH_3OH$ (D_2) is shown in Fig. 1. The D_2 structure crystallizes as a trinuclear cluster in the monoclinic space group ($P2_1$). The

central Fc dicarboxylic acid is connected to two Ag(I) centers through both oxygens of the carboxylic functional group, with Ag⋯O contacts ranging from 2.389 to 2.544 Å (average 2.4515 Å). Each silver atom is connected to two PPh_3 groups, and the Ag–P bond distances vary from 2.425 to 2.440 Å. The Tolman's cone angles in the PPh_3 moiety are in the range of 48.71 to 56.91 degrees which are greater than those in cluster D_1 and can be attributed to the lower steric hindrance. Also, the torsion angles of the cyclopentadienyl rings vary from about 103.67 to 104.97 degrees. Hydrogen bonding between hydrogens of the CH_3OH solvent and the coordinated oxygen of the Fc dicarboxylic acid moiety lead to the presence of methanol in the structure. Generally, the single-crystal X-ray analysis results show that the ferrocenyl group is placed at

the core of the binuclear silver cluster. Related crystallographic data, data refinement, and data on selected bond lengths and angles for cluster D_2 are provided in Tables S1 and S3.† The IR spectrum of D_2 displays characteristic bands at around 3398, 3050, 1544, 1480, 1434, 1383, 746 and 134 cm^{-1} which, due to structural similarities, are quite comparable to those in the IR spectrum of D_1 and are consistent with its formulation (Fig. 2A).

Similar to the results for cluster D_1, the TG curves of D_2 exhibit two weight-loss steps. The cluster loses the CH_3OH molecules below 120 °C (calculated 6.8%, found approx. 6%). After loss of the solvent, the structure is stable until 220 °C. For the D_2 cluster, the main weight-loss step occurs between 220 and 285 °C and can be attributed to the decomposition of the complex (Fig. 2B). Following the main weight-loss step, about 15% further weight is lost between 300 and 800 °C which shows that the organic portion has fully decomposed. Therefore, the remaining part (about 20%) is probably $Ag_2O \cdot FeO$, but it should be noted that no further phase studies on the residuals were performed. The major weight loss of about 75% in the temperature range of 220–800 °C is near to the calculated amount. As a result, during the major weight-loss step, cluster D_2 is fully decomposed to an uncertain metallic structure according to the TGA results. Therefore, D_2 is sufficiently stable for use as a dye degradation photocatalyst with sunlight irradiation.

The pH of the solution is one of the most important factors affecting the adsorption and degradation of dyes because it directly affects the redox reversibility of photocatalysts. The pH values of D_1 and D_2 mixtures with MB without any manipulation are 5.5, so the pH was adjusted to more basic and acidic values (pH = 4 and 7) by the addition of some drops of 0.1 M solutions of NaOH or HNO_3. Any structural changes were followed by PXRD measurements. As shown in Fig. 2C and D, the structures remain unchanged in the mentioned pH range. Therefore, to find the optimum pH value

for the dye degradation reaction, the process of dye degradation was performed in the presence of photocatalyst, hydrogen dioxide and sunlight at different pH values. It should be noted that both D_1 and D_2 samples were kept in darkness for 30 min prior to the experiments and then aliquots were taken from the reaction vessels every 10 min. UV-vis analysis was used to determine the quantity of residual dye in each case. As can be seen in Fig. 3, although the degradation rate is higher at lower pH, the results are similar and so we chose the unchanged pH (5.5) for further degradation studies. The difference in the adsorption behavior of the two compounds at different pHs can be attributed to the presence of a free carbonyl group in D_1, which can interact with H^+ in acidic conditions, reducing available groups for dye adsorption.

As can be seen, the D_1 cluster is better at adsorbing the dye than the D_2 cluster. These findings indicate that D_1 has better interactions with the dye through the non-coordinated oxygens of the carboxylic acid of the $Fc(COO)_2$ moieties. The probable interactions of MB with D_1 could include π–π interactions and hydrogen bonding between the free oxygen of the carbonyl groups and hydrogens of the dye, as shown in Scheme 1.

The as-prepared clusters were employed as photocatalysts for the photodegradation of MB in the presence of H_2O_2 and sunlight. To examine the roles played by various factors such as the H_2O_2, clusters, and sunlight irradiation, seven experimental conditions were applied to both of the clusters: (A) H_2O_2/dark, (B) photocatalyst/dark, (C) H_2O_2/photocatalyst/dark, (D) irradiation only, (E) H_2O_2/irradiation, (F) photocatalyst/irradiation, and (G) photocatalyst/irradiation/H_2O_2. As can be seen in Fig. 4, the best degradation of the model dye is achieved by the simultaneous addition of H_2O_2 and D_1 with sunlight irradiation. Also, the degradation rate of H_2O_2/photocatalyst/irradiation is better than that achieved without light irradiation. With continuous irradiation for about 15
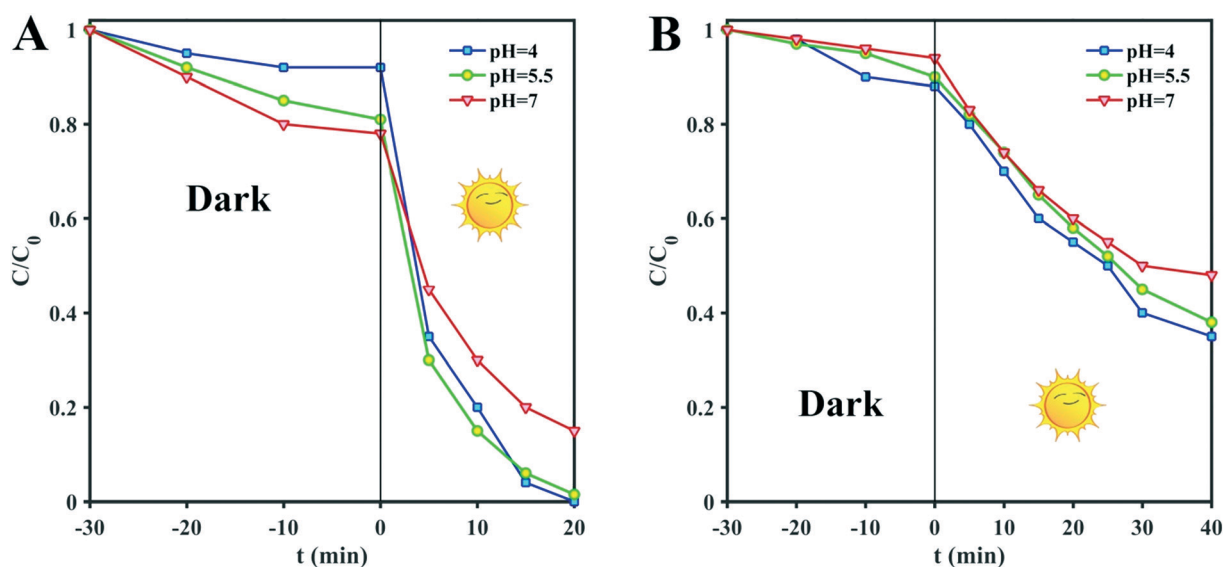

Fig. 3 Percentages of MB remaining in aqueous solutions over time in the presence of H_2O_2/photocatalyst/sunlight at different pH values. Part A corresponds to D_1 and part B corresponds to D_2; 100 mL of 150 ppm MB was used in each experiment.
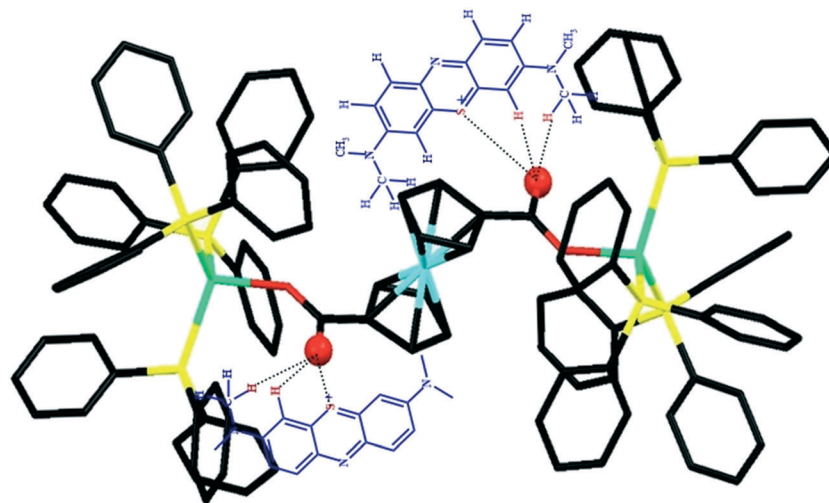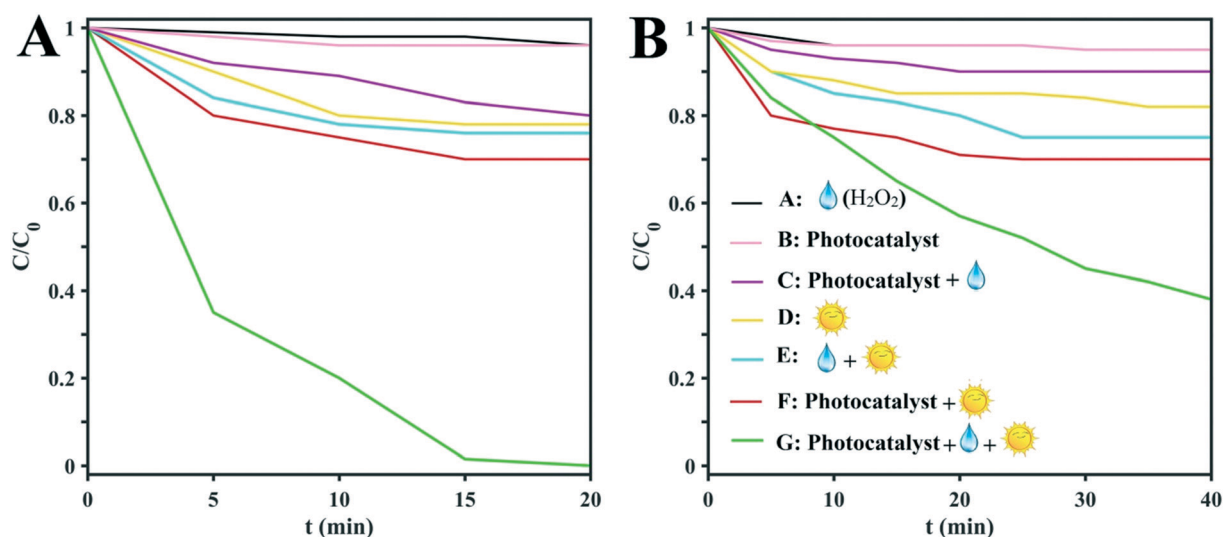
Scheme 1 Probable interactions between D_1 and MB.

Fig. 4 Degradation over time of MB (as a model dye) under different conditions by D_1 (A) and D_2 (B). Black lines: H_2O_2/dark; pink lines: photocatalyst/dark; purple lines: H_2O_2/photocatalyst/dark; yellow lines: irradiation only; cyan lines: H_2O_2/irradiation; red lines: photocatalyst/irradiation; green lines: H_2O_2/photocatalyst/irradiation.

min, the colors of the MB solutions disappear, which means that the dye molecules have degraded. Quantitative determinations of the photodegradation rates were obtained from $\ln(C/C_0)$ *vs.* time plots (Fig. 4A and B) based on the peak intensities of the UV-vis spectra (664 nm).

The UV-vis spectra in Fig. 5 compare the degradation achieved over time by the D_1 (A) and D_2 (B) catalysts with H_2O_2 and irradiation. The UV-vis peak at 664 nm is very strong for the MB solution without photodegradation. The results show that in the presence of D_1, the photodegradation rate of the dye is clearly accelerated. The decrease in dye concentration is obvious after 5 min and the concentration reaches zero after less than 20 min of irradiation. Clearly, D_2 shows a lower photocatalytic capacity for the degradation of MB in comparison with D_1. The gradual decrease in the UV-vis

vis spectral intensity and accompanying fading colors of the model dye solutions prove that D_2 is a weaker photocatalyst. The pictures of the dye solutions obviously show that the color of MB fades more slowly during the reaction with D_2 in comparison to that with D_1.

The linear plots of $\ln(C/C_0)$ *vs.* time for all of the degradation processes are consistent with the first-order kinetic equation (Fig. S1†). The results confirm that D_1 is an extraordinary catalyst for MB photodegradation under sunlight irradiation. The linear fitting shows a rate constant of about $\sim$0.24 s^{-1} for MB degradation catalyzed by D_1. The rate constant is about ten times lower for D_2 ($\sim$0.024 s^{-1}) indicating that the photocatalytic performance of D_2 as the MB degradation photocatalyst is limited in comparison with that of D_1. However, it is still more efficient than many MB degradation
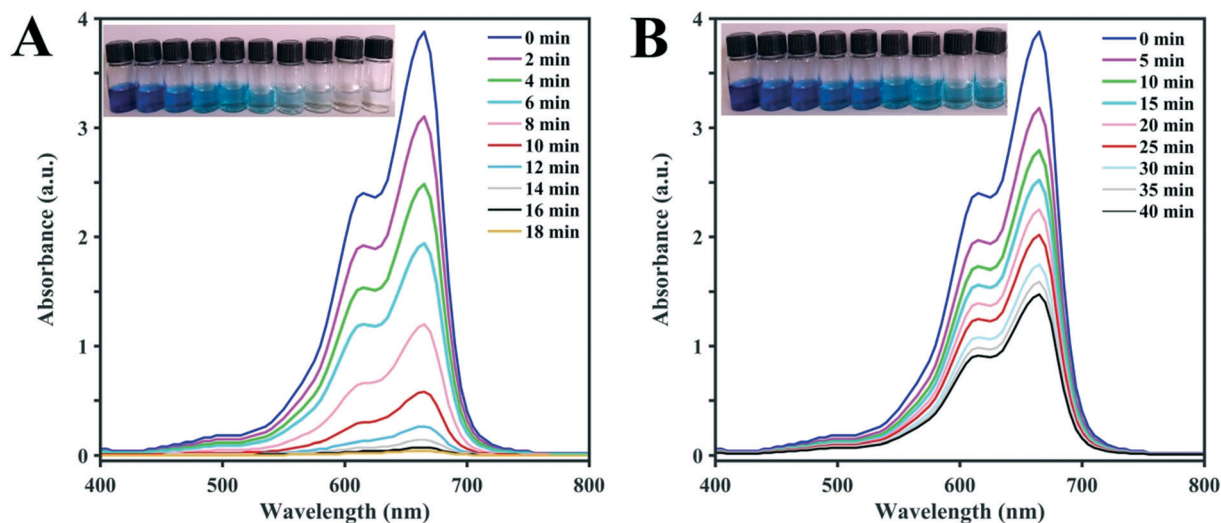
Fig. 5 The pictures and corresponding UV-vis spectra of MB solutions after photodegradation with visible light ($\lambda > 420$ nm) for different times using (A) D_1 and (B) D_2 clusters as the photocatalysts.

photocatalysts. The degradation efficiencies of D_1 and D_2 toward MB are about 1500 mg g^{-1} and 900 mg g^{-1} which are far greater than those of other reported catalysts.[29–32] It should be noted that the MB degradation rate of D_1 is very high and only 10 mg of D_1 can decolorize more than 100 mL of a 150 ppm MB solution in less than 20 min. In other words, it can be said that the rate of color destruction by this structure is equal to 75 mg g^{-1} min^{-1}, which is unique.

It is clear that the photocatalytic efficiency of D_1 under sunlight irradiation toward MB is better than that of D_2 and it is assumed that it may involve semi-conductivity. Based on recent studies, structures formed by metals with variable valences due to their semi-conductive nature may act as photocatalysts.[33] Consequently, UV-vis diffuse reflectance spectroscopy (DRS) was employed to investigate the optical natures of the structures. The strong broad absorption band of the

two clusters in the range of 200 to 300 nm shown in Fig. 6A reduces distinctly beyond 360 nm in the UV region. On the other hand, there is a strong broad absorption band in the visible region (380 to 580 nm). The high absorbance intensity of both structures (up to 800 nm) in the visible range over the entire visible spectrum has great importance. As seen in Fig. 6B, the bandgap of the structures can be evaluated from UV-vis DRS based on the Kubelka–Munk function. Due to the high structural similarity of the compounds, the values of the bandgaps (E_g) are very close to each other and are about 2 eV (obtained from the intersection points of the absorption edges in plots of F against E). These values reveal that the D_1 and D_2 clusters could act as excitable semi-conductors in visible light and that their photocatalytic performances could be a consequence of the visible and UV light in the sunlight.
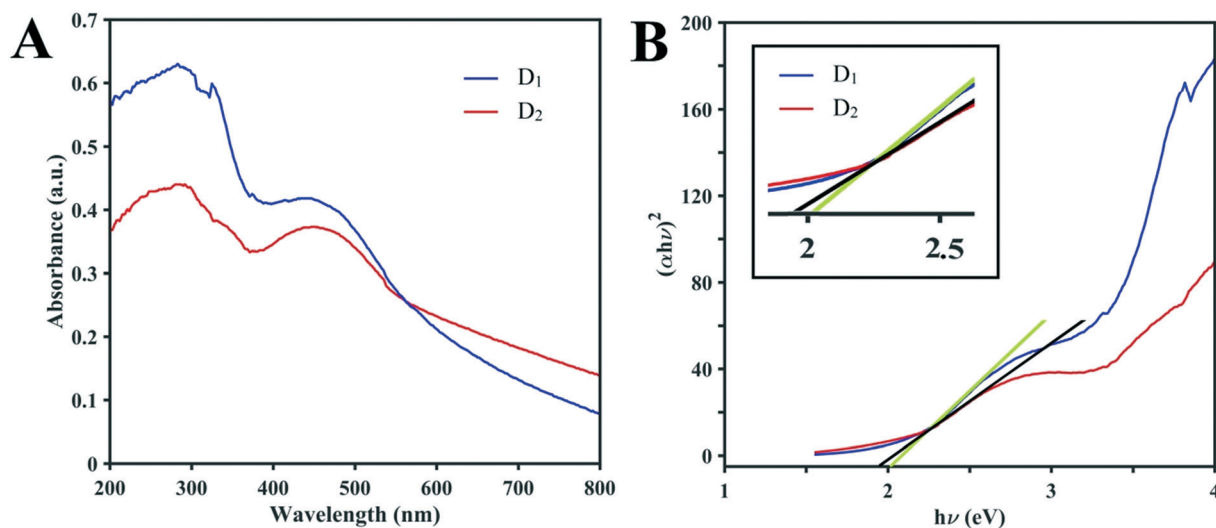

Fig. 6 (A) Solid-state UV-vis absorption spectra of D_1 and D_2 at ambient temperature. (B) Curves of the Kubelka–Munk function *vs. E* for D_1 and D_2 (the inset shows the magnification).

To evaluate the activation energy (E_a) of dye degradation, the process was performed at various temperatures in the temperature range of 10–40.5 °C using a water bath. The collected data are shown in Fig. 7. The k_0 value increases slowly with increasing reaction temperature. From Fig. 7, it can be seen that $\ln(k_0)$ shows a linear dependence on T^{-1}, indicating that the Arrhenius equation governs the reaction rate:
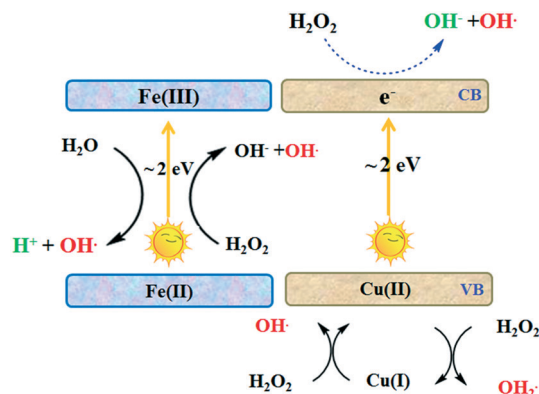
$$\ln k = \ln A - \frac{E_a}{RT} \tag{1}$$

where A and R denote the pre-exponential factor and molar gas constant, respectively, and the activation energy is E_a. The relatively small value of E_a signifies that the MB photocatalytic degradation could be based on a free radical mechanism because it is less than a typical activation energy for the direct cleavage of chemical bonds.

Proposed mechanism

The structural similarity of D_1 and D_2 is due to the presence of the Fc group. Fc is a transition metal compound ($Fe(C_5H_5)_2$), which possesses an electron donor–acceptor conjugated structure, and presents good reversible redox features.[33] Cyclic voltammetry (CV) experiments confirm electron transfer during the reaction.[34–39] Thus, the Fc moiety may be oxidized to its cationic form (Fc^+) and subsequently restored by an electron shift which produces the hydroxyl radical through the conversion of Fe(II) to Fe(III) in the presence of H_2O_2 (Fig. S2†).

Comparative investigations using scavengers were done to estimate the principal active species involved in dye degradation. Appropriate quenchers of oxidative intermediates (oxygen or hydroxyl radicals) were added to examine the possibility of their formation.[40] KI was applied as the OH radical quencher and NaN_3 was used for the elimination of oxygen

Scheme 2 The proposed mechanism of MB degradation by the photocatalyst D_1 cluster under sunlight illumination in the presence of H_2O_2.

and OH radical. Fig. S3† shows that the fading of the blue color reduces from 100 to 82% after the addition 0.25 mM of NaN_3, and drops to 77% when the concentration of NaN_3 is increased to 0.5 mM. The 18% of color was remained by using 0.25 KI and that even reduced to 7% in the presence of 0.5 mM KI as a radical scavenger. Furthermore, it can be proved that both oxygen and ·OH contribute to the dye discoloration, but it is clear that ·OH has the primary effect and plays the main role. Monitoring of the pH values during the photocatalytic process showed that the pH of the reaction vessel remains largely unchanged. So, the possible reaction mechanism for the Fc portion of the structures is proposed to be as follows:[41]
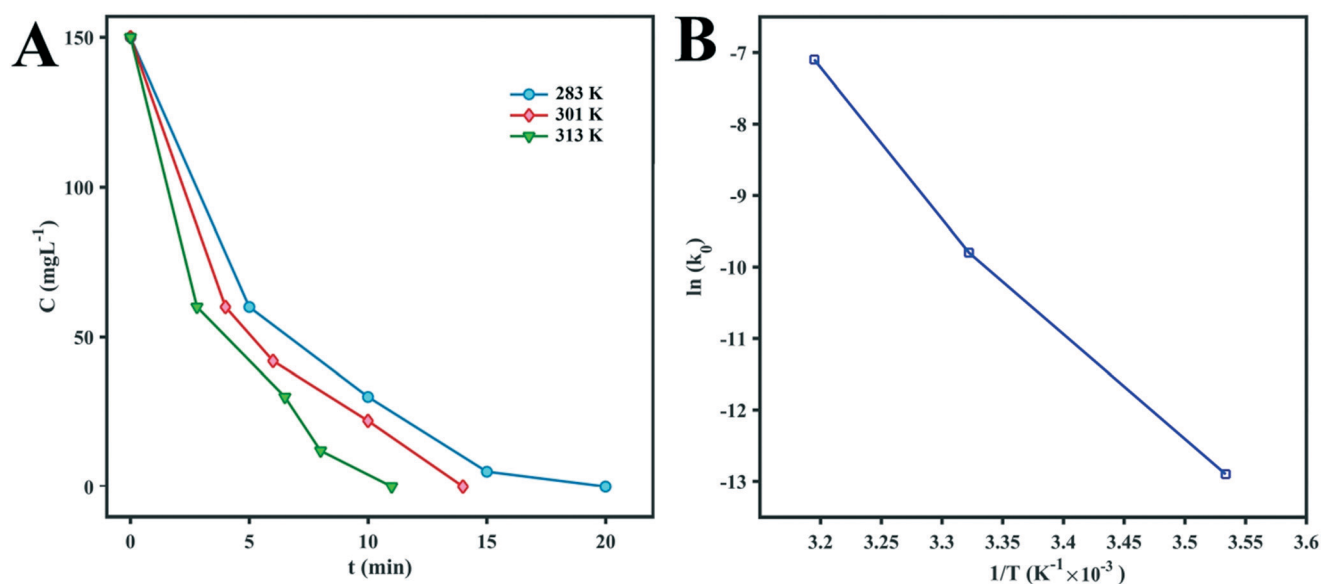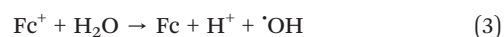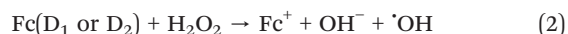
$$Fc(D_1 \text{ or } D_2) + H_2O_2 \rightarrow Fc^+ + OH^- + {}^\bullet OH \tag{2}$$

$$Fc^+ + H_2O \rightarrow Fc + H^+ + {}^\bullet OH \tag{3}$$

Fig. 7 (A) Kinetic curves of MB degradation at different temperatures. (B) Arrhenius plot of $\ln(k_0)$ vs. $(1/T)$ for the photocatalytic degradation of MB by D_1.
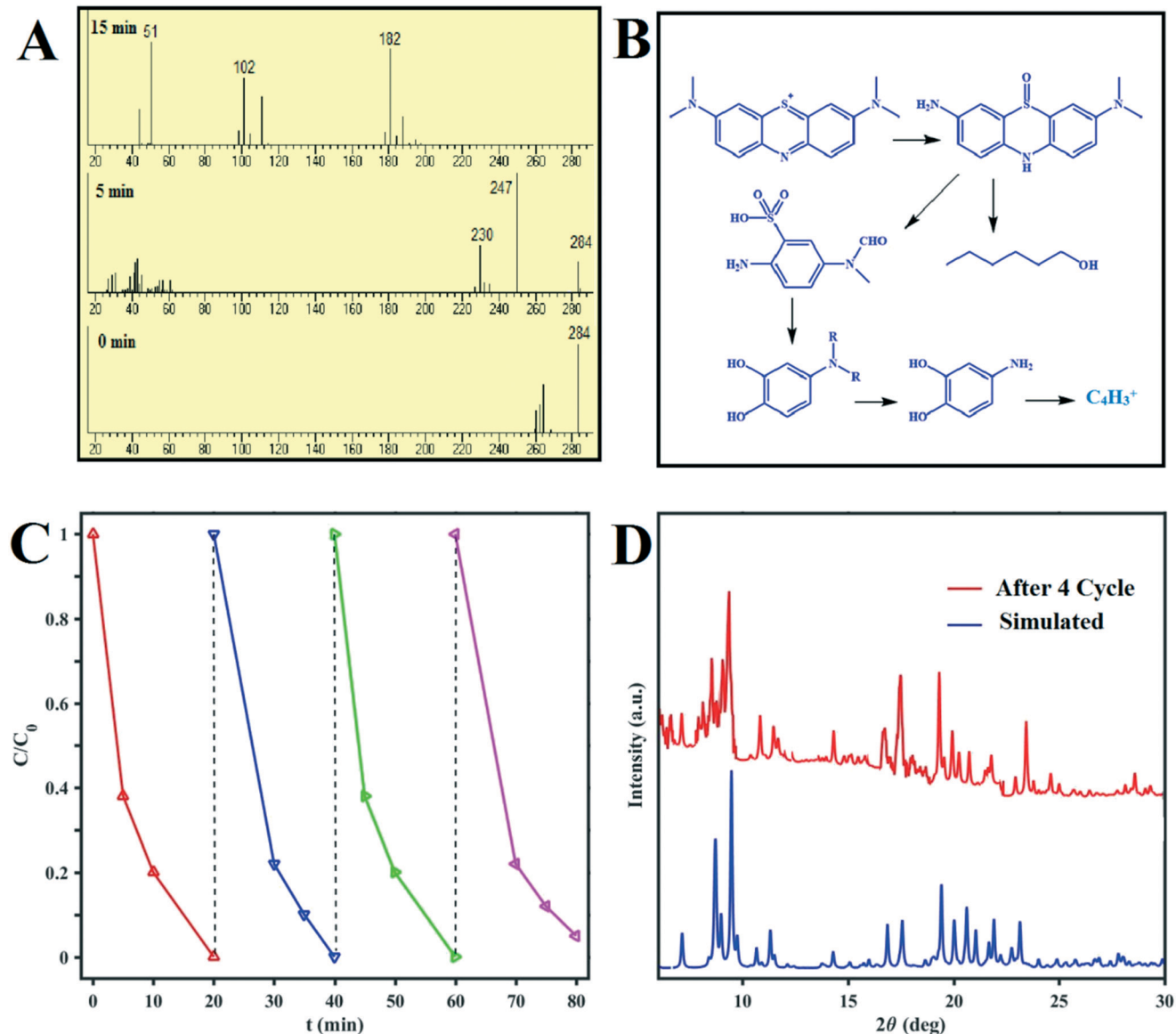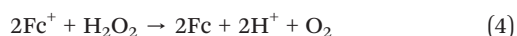
Fig. 8 (A) Mass spectra recorded of MB degradation at different reaction times. (B) Photocatalytic degradation pathway of MB.[19] (C) Recycling tests using D_1 under sunlight irradiation for the photocatalytic degradation of MB. (D) Powder XRD patterns of D_1 before and after four MB photocatalytic degradation cycles.

$$2Fc^+ + H_2O_2 \rightarrow 2Fc + 2H^+ + O_2 \qquad (4)$$

The obtained high photocatalytic degradation efficiency of MB by D_1 confirms however that another mechanism is incorporated in the dye degradation.

Based on the literature, illumination of the mixture of dye and photocatalysts by light or photons with equal or greater energy than the photocatalyst bandgap can excite some electrons from the photocatalyst VB to the CB and create holes (h^+) in the VB. Although extensive studies have confirmed that organic linkers can serve as the VB and the metallic portion can act as the CB, here it seems that the Cu ions and ligands play the roles of VB and CB, respectively. However, due to the relatively low standard electrochemical
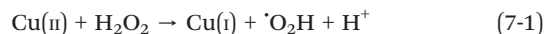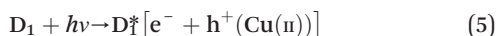
potential of Cu(II) to Cu(I) (0.159 V), the Cu(I) in D_1 can be easily converted to Cu(II).

As shown in eqn (6), H_2O_2 (as an effective electron scavenger) can be combined with an electron to form $^•OH$ and OH^-. On the other hand, the stabilization of formed holes (Cu(II)) can be achieved by bonding with generated hydroxides (eqn (6)) or other oxygen-containing moieties or solvents in the reaction vessel.

As shown in eqn (7-1) and (7-2), Fenton-like reactions may occur based on *in situ* formed Cu(II) to create more $^•OH$ species. By adding dye to the reaction vessel, consumption of $^•OH$ during the dye degradation drives eqn (2)–(4), leading to the formation of more Cu(II) and hydroxyl (^-OH) species.

The probable photocatalytic mechanism is presented in Scheme 2. It should be noted that other mechanisms, such

as (A) homolytic cleavage of H_2O_2 following irradiation; (B) oxidation of the Cu(I)/Cu(II) in the presence of H_2O_2, and therefore progress of the Fenton-like process; and (C) engagement of O_2, are also probable although they seem to have less effect in comparison to the suggested mechanism; they may play roles in the lower-efficiency removal of dyes in the absence of light or H_2O_2. Thus, the superb performance of D_1 is due to a combination of Fenton and Fenton-like mechanisms as schematically illustrated in Scheme 2.

$$D_1 + h\nu \rightarrow D_1^* \left[e^- + h^+(Cu(II))\right] \tag{5}$$

$$H_2O_2 + e^- \rightarrow {}^{\cdot}OH + OH^- \tag{6}$$

$$Cu(II) + H_2O_2 \rightarrow Cu(I) + {}^{\cdot}O_2H + H^+ \tag{7-1}$$

$$Cu(I) + H_2O_2 \rightarrow Cu(II) + OH^- + {}^{\cdot}OH \tag{7-2}$$

It should be noted that the ability to use a Cu-based Fenton-like catalyst in a neutral solution is a significant advantage. Furthermore, the change in the pH value of the reaction vessel during the degradation of MB is less than 0.5 units.[42,43]

Analysis of MB degradation products during the photocatalytic reaction and reusability of D_1

The intermediates and final products of the MB degradation reactions were analyzed by mass spectroscopy. The supernatants of the dye solutions at different times during the degradation process and their mass patterns are presented in Fig. 8. Based on the obtained results, the main metabolites of MB were identified and reported based on their molecular weights; these confirm the effectiveness of the designed photocatalysts for MB degradation under sunlight irradiation. MB photodegradation cycling experiments were carried out using D_1 as the photocatalyst to test its stability. As shown in Fig. 8C, no obvious drop in the photocatalytic performance of D_1 is recognized after four cycles of the reaction. Moreover, the XRD pattern of D_1 after four photodegradation cycles presented in Fig. 8D proves its structural stability.

Conclusion

Two novel Fc-functionalized coinage clusters $[(PPh_3)_3CuO_2\text{-}CFcCO_2Cu(PPh_3)_3]\cdot3CH_3OH$ (D_1) and $[(PPh_3)_2AgO_2CFcCO_2Ag(PPh_3)_2]_2\cdot7CH_3OH$ (D_2) were designed and synthesized for dye degradation by concurrent heterogenic Fenton and Fenton-like reactions under natural sunlight. The results show that the degradation efficiencies of D_1 and D_2 toward MB are about 1500 mg g^{-1} and 900 mg g^{-1}, respectively, which are far higher than those of other reported catalysts. It should be noted that the MB degradation rate of D_1 is very high and only 10 mg of D_1 can decolorize more than 100 mL of a 150 ppm MB solution in about 15 min. Furthermore, the performance of D_1 as a dual photocatalyst under natural sunlight irradiation in the presence of H_2O_2 does not need any pH adjustment which is a unique feature of this photocatalyst. The

difference between the photocatalytic performances of D_1 and D_2, which are structurally very similar, shows that the combination of Fenton and Fenton-like mechanisms in heterogenic clusters could be a very promising method for dye degradation in natural sunlight.

Conflicts of interest

There are no conflicts to declare.

Acknowledgements

References

1 M. B. Ahmed, J. L. Zhou, H. H. Ngo, W. Guo, N. S. Thomaidis and J. Xu, Progress in the biological and chemical treatment technologies for emerging contaminant removal from wastewater: a critical review, *J. Hazard. Mater.*, 2017, **323**, 274–298.

2 S. Arslan, M. Eyvaz, E. Gürbulak and E. Yüksel, *A Review of State-of-the-Art Technologies in Dye-Containing Wastewater Treatment–The Textile Industry Case, Textile Wastewater Treatment*, 2016.

3 S. Ghosh, N. A. Kouamé, L. Ramos, S. Remita, A. Dazzi, A. Deniset-Besseau, P. Beaunier, F. Goubard, P.-H. Aubert and H. Remita, Conducting polymer nanostructures for photocatalysis under visible light, *Nat. Mater.*, 2015, **14**, 505.

4 C. Lu, P. Zhang, S. Jiang, X. Wu, S. Song, M. Zhu, Z. Lou, Z. Li, F. Liu and Y. Liu, Photocatalytic reduction elimination of UO22+ pollutant under visible light with metal-free sulfur doped g-C3N4 photocatalyst, *Appl. Catal., B*, 2017, **200**, 378–385.

5 L. Xu, L. Cheng, C. Wang, R. Peng and Z. Liu, Conjugated polymers for photothermal therapy of cancer, *Polym. Chem.*, 2014, **5**, 1573–1580.

6 K. Yang, H. Xu, L. Cheng, C. Sun, J. Wang and Z. Liu, In vitro and in vivo near-infrared photothermal therapy of cancer using polypyrrole organic nanoparticles, *Adv. Mater.*, 2012, **24**, 5586–5592.

7 Q. Chen, Q. He, M. Lv, Y. Xu, H. Yang, X. Liu and F. Wei, Selective adsorption of cationic dyes by UiO-66-NH2, *Appl. Surf. Sci.*, 2015, **327**, 77–85.

8 F. Rouhani, A. Morsali and P. Retailleau, Simple One-Pot Preparation of a Rapid Response AIE Fluorescent Metal–Organic Framework, *ACS Appl. Mater. Interfaces*, 2018, **10**(42), 36259–36266.

9 A. K. Verma, R. R. Dash and P. Bhunia, A review on chemical coagulation/flocculation technologies for removal of colour from textile wastewaters, *J. Environ. Manage.*, 2012, **93**, 154–168.

10 F. Rouhani, F. Rafizadeh-Masuleh and A. Morsali, Selective sacrificial metal–organic frameworks: a highly quantitative colorimetric naked-eye detector for aluminum ions in aqueous solutions, *J. Mater. Chem. A*, 2019, **7**, 18634–18641.

11 F. Rouhani and A. Morsali, Goal-Directed Design of Metal–Organic Frameworks for HgII and PbII Adsorption from Aqueous Solutions, *Chem. – Eur. J.*, 2018, **24**, 17170–17179.

12 F. Rouhani and A. Morsali, Fast and Selective Heavy Metal Removal by a Novel Metal-Organic Framework Designed with In-Situ Ligand Building Block Fabrication Bearing Free Nitrogen, *Chem. – Eur. J.*, 2018, **24**, 5529–5537.

13 X. Sheng, Y. Liu, Y. Wang, Y. Li, X. Wang, X. Wang, Z. Dai, J. Bao and X. Xu, Cesium Lead Halide Perovskite Quantum Dots as a Photoluminescence Probe for Metal Ions, *Adv. Mater.*, 2017, **29**, 1700150.

14 R. Tovar-Gomez, D. Rivera-Ramírez, V. Hernandez-Montoya, A. Bonilla-Petriciolet, C. Durán-Valle and M. Montes-Morán, Synergic adsorption in the simultaneous removal of acid blue 25 and heavy metals from water using a Ca(PO$_3$) 2-modified carbon, *J. Hazard. Mater.*, 2012, **199**, 290–300.

15 H. Zhang, X. Wang, Q. Liao, Z. Xu, H. Li, L. Zheng and H. Fu, Embedding perovskite nanocrystals into a polymer matrix for tunable luminescence probes in cell imaging, *Adv. Funct. Mater.*, 2017, **27**, 1604382.

16 K.-G. Liu, F. Rouhani, Q.-D. Shan, R. Wang, J. Li, M.-L. Hu, X. Cheng and A. Morsali, Ultrasonic-assisted fabrication of thin-film electrochemical detector of H$_2$O$_2$ based on ferrocene-functionalized silver cluster, *Ultrason. Sonochem.*, 2019, **56**, 305–312.

17 S. I. Liochev, The mechanism of "Fenton-like" reactions and their importance for biological systems. A biologist's view, in *Metal ions in biological systems*, Routledge, 2018, pp. 1–39.

18 X. Liu, Y. Zhou, J. Zhang, L. Luo, Y. Yang, H. Huang, H. Peng, L. Tang and Y. Mu, Insight into electro-Fenton and photo-Fenton for the degradation of antibiotics: Mechanism study and research gaps, *Chem. Eng. J.*, 2018, **347**, 379–397.

19 H.-H. Huang, M.-C. Lu and J.-N. Chen, Catalytic decomposition of hydrogen peroxide and 2-chlorophenol with iron oxides, *Water Res.*, 2001, **35**, 2291–2299.

20 R. L. Valentine and H. A. Wang, Iron oxide surface catalyzed oxidation of quinoline by hydrogen peroxide, *J. Environ. Eng.*, 1998, **124**, 31–38.

21 C. K.-J. Yeh, W.-S. Chen and W.-Y. Chen, Production of hydroxyl radicals from the decomposition of hydrogen peroxide catalyzed by various iron oxides at pH 7, *Pract. Period. Hazard., Toxic, Radioact. Waste Manage.*, 2004, **8**, 161–165.

22 M. Cheng, W. Ma, J. Li, Y. Huang, J. Zhao, Y. X. Wen and Y. Xu, Visible-light-assisted degradation of dye pollutants over Fe (III)-loaded resin in the presence of H2O2 at neutral pH values, *Environ. Sci. Technol.*, 2004, **38**, 1569–1575.

23 A. Georgi, A. Schierz, U. Trommler, C. Horwitz, T. Collins and F.-D. Kopinke, Humic acid modified Fenton reagent for enhancement of the working pH range, *Appl. Catal., B*, 2007, **72**, 26–36.

24 A. Kumar, A. Rana, G. Sharma, M. Naushad, P. Dhiman, A. Kumari and F. J. Stadler, Recent advances in nano-Fenton catalytic degradation of emerging pharmaceutical contaminants, *J. Mol. Liq.*, 2019, 111177.

25 J. Tan, H. Li, X. Hu, R. Abdullah, S. Xie, L. Zhang, M. Zhao, Q. Luo, Y. Li and Z. Sun, Size-tunable assemblies based on ferrocene-containing DNA polymers for spatially uniform penetration, *Chem*, 2019, **5**, 1687–1689.

26 Q. Wang, S. Tian and P. Ning, Ferrocene-Catalyzed heterogeneous fenton-like degradation of methylene blue: influence of initial solution pH, *Ind. Eng. Chem. Res.*, 2014, **53**, 6334–6340.

27 F. Rouhani, F. Rafizadeh-Masuleh and A. Morsali, Highly Electro-Conductive Metal-Organic Framework; Tunable by Metal Ion Sorption Quantity, *J. Am. Chem. Soc.*, 2019, **141**, 11173–11182.

28 C. Minero, M. Lucchiari, D. Vione and V. Maurino, Fe (III)-enhanced sonochemical degradation of methylene blue in aqueous solution, *Environ. Sci. Technol.*, 2005, **39**, 8936–8942.

29 Y. He, D. B. Jiang, J. Chen, D. Y. Jiang and Y. X. Zhang, Synthesis of MnO$_2$ nanosheets on montmorillonite for oxidative degradation and adsorption of methylene blue, *J. Colloid Interface Sci.*, 2018, **510**, 207–220.

30 A. Ivanets, M. Roshchina, V. Srivastava, V. Prozorovich, T. Dontsova, S. Nahirniak and M. Sillanpää, Effect of metal ions adsorption on the efficiency of methylene blue degradation onto MgFe$_2$O$_4$ as Fenton-like catalysts, *Colloids Surf., A*, 2019, **571**, 17–26.

31 J. T. Adeleke, T. Theivasanthi, M. Thiruppathi, M. Swaminathan, T. Akomolafe and A. B. Alabi, Photocatalytic degradation of methylene blue by ZnO/NiFe$_2$O$_4$ nanoparticles, *Appl. Surf. Sci.*, 2018, **455**, 195–200.

32 C. H. Nguyen, C. C. Fu and R. S. Juang, Degradation of methylene blue and methyl orange by palladium-doped TiO$_2$ photocatalysis for water reuse: Efficiency and degradation pathways, *J. Cleaner Prod.*, 2018, **202**, 413–427.

33 P. Štěpnička, J. Demel and J. Čejka, Preparation and catalytic application of MCM-41 modified with a ferrocene carboxyphosphine and a ruthenium complex, *J. Mol. Catal. A: Chem.*, 2004, **224**, 161–169.

34 Q. Wang, S. Tian, J. Cun and P. Ning, Degradation of methylene blue using a heterogeneous Fenton process catalyzed by ferrocene, *Desalin. Water Treat.*, 2013, **51**, 5821–5830.

35 F. Rouhani, B. Gharib and A. Morsali, Solvent switching smart metal–organic framework as a catalyst of reduction and condensation, *Inorg. Chem. Front.*, 2019, **6**, 2412–2422.

36 J. Kim, F. Martinez and I. Metcalfe, The beneficial role of use of ultrasound in heterogeneous Fenton-like system over supported copper catalysts for degradation of p-chlorophenol, *Catal. Today*, 2007, **124**, 224–231.

37 F. L. Lam, A. C. Yip and X. Hu, Copper/MCM-41 as a highly stable and pH-insensitive heterogeneous photo-Fenton-like catalytic material for the abatement of organic wastewater, *Ind. Eng. Chem. Res.*, 2007, **46**, 3328–3333.

38 H.-J. Lee, H. Lee and C. Lee, Degradation of diclofenac and carbamazepine by the copper (II)-catalyzed dark and photo-assisted Fenton-like systems, *Chem. Eng. J.*, 2014, **245**, 258–264.

39 X.-J. Huang, H.-S. Im, D.-H. Lee, H.-S. Kim and Y.-K. Choi, Ferrocene functionalized single-walled carbon nanotube bundles. Hybrid interdigitated construction film for L-glutamate detection, *J. Phys. Chem. C*, 2007, **111**, 1200–1206.

40 W. Li, S. Zhao, B. Qi, Y. Du, X. Wang and M. Huo, Fast catalytic degradation of organic dye with air and MoO3: Ce nanofibers under room condition, *Appl. Catal., B*, 2009, **92**, 333–340.

41 M. A. Shannon, P. W. Bohn, M. Elimelech, J. G. Georgiadis, B. J. Marinas and A. M. Mayes, Science and technology for water purification in the coming decades, in *Nanoscience and technology: a collection of reviews from nature Journals*, World Scientific, 2010, pp. 337–346.

42 Y. Feng, H. Lu, X. Gu, J. Qiu, M. Jia, C. Huang and J. Yao, ZIF-8 derived porous N-doped ZnO with enhanced visible light-driven photocatalytic activity, *J. Phys. Chem. Solids*, 2017, **102**, 110–114.

43 C. Zhang, L. Ai and J. Jiang, Graphene hybridized photoactive iron terephthalate with enhanced photocatalytic activity for the degradation of rhodamine B under visible light, *Ind. Eng. Chem. Res.*, 2014, **54**, 153–163.

This journal is © The Royal Society of Chemistry 2020

Catal. Sci. Technol., 2020, **10**, 757–767 | **767**